

MODIFICATIONS OF 2:1 CLAY MINERALS IN A KAOLINITE-DOMINATED ULTISOL UNDER CHANGING LAND-USE REGIMES

JASON C. AUSTIN^{1,2}, AMELIA PERRY², DANIEL D. RICHTER¹, AND PAUL A. SCHROEDER²

¹ Duke University, Nicholas School of the Environment, Durham, NC 27708-0328 USA

² University of Georgia, Department of Geology, Athens, GA 30602-2501 USA

Abstract—Chemical denudation and chemical weathering rates vary under climatic, bedrock, biotic, and topographic conditions. Constraints for landscape evolution models must consider changes in these factors on human and geologic time scales. Changes in nutrient dynamics, related to the storage and exchange of K^+ in clay minerals as a response to land use change, can affect the rates of chemical weathering and denudation. Incorporation of these changes in landscape evolution models can add insight into how land use changes affect soil thickness and erodibility. In order to assess changes in soil clay mineralogy that result from land-use differences, the present study contrasts the clay mineral assemblages in three proximal sites that were managed differently over nearly the past two centuries where contemporary vegetation was dominated by old hardwood forest, old-field pine, and cultivated biomes. X-ray diffraction (XRD) of the oriented clay fraction using K-, Mg-, and Na-saturation treatments for the air-dried, ethylene glycol (Mg-EG and K-EG) solvated, and heated (100, 350, and 550°C) states were used to characterize the clay mineral assemblages. XRD patterns of degraded biotite (oxidized Fe and expelled charge-compensating interlayer K) exhibited coherent scattering characteristics similar to illite. XRD patterns of the Mg-EG samples were, therefore, accurately modeled using NEWMOD2[®] software by the use of mineral structure files for discrete illite, vermiculite, kaolinite, mixed-layer kaolinite-smectite, illite-vermiculite, kaolinite-illite, and hydroxy-interlayered vermiculite. The soil and upper saprolite profiles that formed on a Neoproterozoic gneiss in the Calhoun Experimental Forest in South Carolina, USA, revealed a depth-dependence for the deeply weathered kaolinitic to the shallowly weathered illitic/vermiculitic mineral assemblages that varied in the cultivated, pine, and hardwood sites, respectively. An analysis of archived samples that were collected over a five-decade growth period from the pine site suggests that the content of illite-like layers increased at the surface within 8 y. Historical management of the sites has resulted in different states of dynamic equilibrium, whereby deep rooting at the hardwood and pine sites promotes nutrient uplift of K from the weathering of orthoclase and micas. Differences in the denudation rates at the cultivated, pine, and hardwood sites through time were reflected by changes in the soil clay mineralogy. Specifically, an increased abundance of illite-like layers in the surface soils can serve as a reservoir of K^+ .

Key Words—Calhoun Experimental Forest, Degraded Biotite, Kaolinitic Ultisol, X-ray Pattern Modeling.

INTRODUCTION

The landscape of the southeastern U.S. Calhoun Critical Zone Observatory (CCZO), located in Union County, South Carolina, USA, was devastated by deforestation and farming practices between the time of colonial settlement (~1700) to the 1930s. Following the collapse of agriculture, pines began to encroach on the previously farmed land and a process of reforestation began. This reforestation process is perceived as a recovery or restoration of normal hydrological and biological cycling in the soil. Observation of the landscape with light detection and ranging (LiDAR) suggests that, in fact, the pines have only served to obscure the changed landscape that has persisted with the attendant hydrologic and biologic changes (NCALM, 2016). By examining soil properties, which include the

clay mineral and nutrient contents, changes to the hydrological and biological cycling can be determined. The present study hypothesized that management by the U.S. Forest Service resulted in a new state of dynamic equilibrium for the critical zone that is dependent on the degree of denudation and the subsequent plant-cover type and management. The present study tested this hypothesis by comparing the clay mineralogy of subsurface <2 μm fractions collected from a hardwood forest that was at least 150 y old (Cook *et al.*, 2015), a loblolly pine (*Pinus taeda*) plot established in 1958 as part of the Calhoun Research Station's Long Term Soil Experiment (LTSE) (Richter and Markewitz, 1995, 2001; Markewitz and Richter, 2000), and a cultivated field managed by the South Carolina Department of Natural Resources that has been under continuous cultivation throughout at least the 20th century (Figure 1). When the Calhoun Critical Zone Observatory was established in 2014, one of its guiding principles was to assess the state of the critical zone relative to the question of "regeneration" vs. the "obscuring" caused by the regrowth of pine forests.

* E-mail address of corresponding author:

jayc.austin@gmail.com

DOI: 10.1346/CCMN.2017.064085

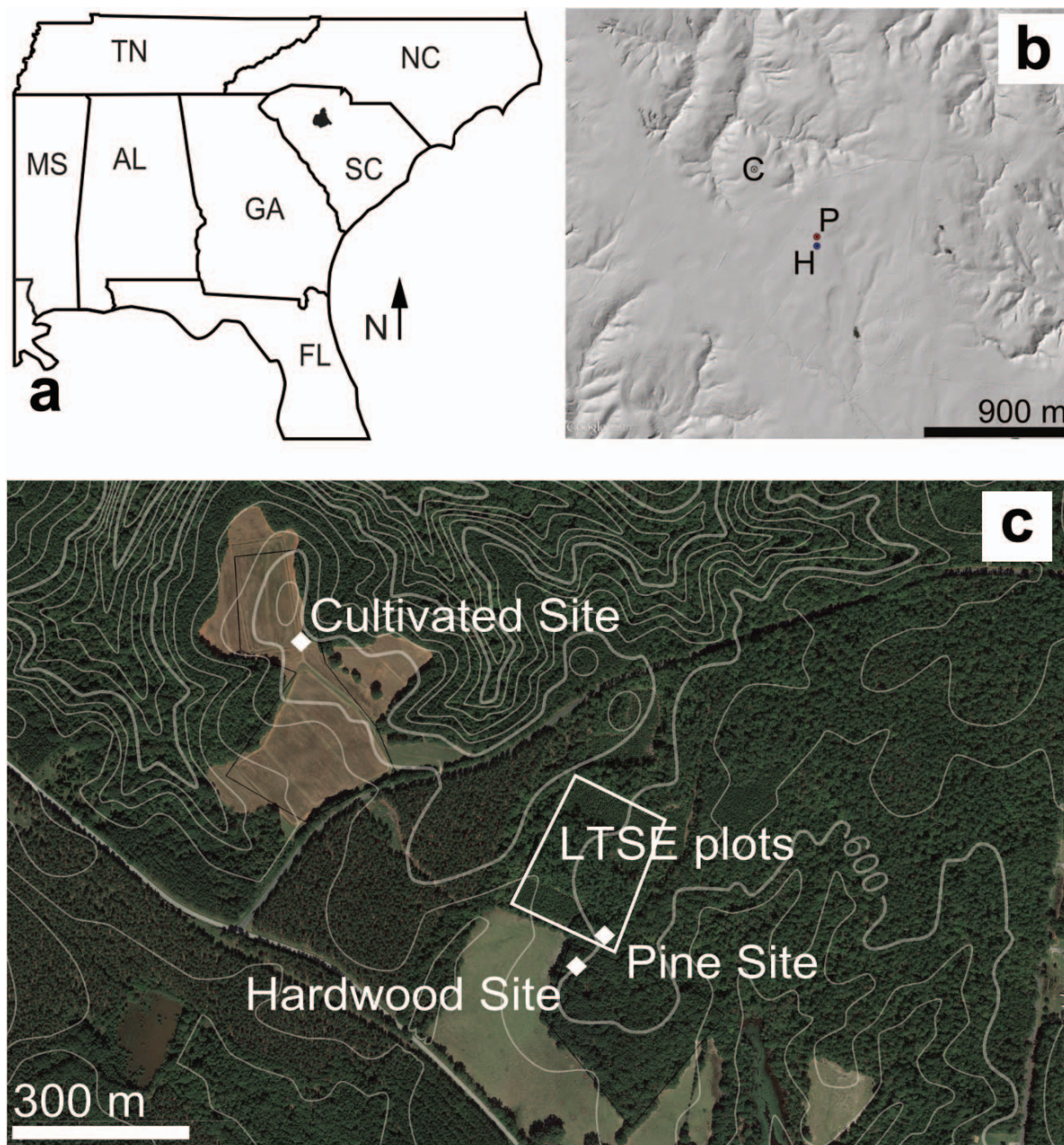


Figure 1. Location of (a) Sumter National Forest in South Carolina, USA; (b) reference area 1 in the Calhoun CZO overlaid with a LiDAR image; and (c) locations of the three soil cores collected from reference area 1 (hardwood and pine sites), the USDA Sedalia Dove Field (cultivated site), and the LTSE plots.

One metric to evaluate the degree of recovery, or the sustainability of the state of the soil and critical zone, is to assess the degree to which the clay mineral assemblages act as reservoirs for the nutrients necessary to sustain plant growth. As defined by Barre *et al.* (2007b), illite-like minerals were identified herein using XRD pattern analyses and no attempt was made to measure layer charge. Illite-like minerals include well and poorly crystallized illites and illite-smectite (IS). Both of these minerals have been shown to act as K^+

reservoirs for soils that control the K^+ concentrations in soil solutions (Barre *et al.*, 2007b, 2008a, 2008b). Barre *et al.* (2007a, 2008a, 2008b) have hypothesized that illite-like minerals in these soils form after the vermiculitization of biotite, where the oxidation of trioctahedral Fe(II) to Fe(III) and the expulsion of K^+ (to compensate a lower layer charge) creates a dioctahedral-like structure. The fixation of available K^+ in vermiculite interlayers may then produce the illite-like components of the clay mineral assemblages (Barre *et*

al., 2007a, 2008a, 2008b). An increased K^+ concentration in soils due to fertilization can be manifested as an increased abundance of illite-like minerals at the expense of expandable layers (Pernes-Debayer *et al.*, 2003; Officer *et al.*, 2006; Barre *et al.*, 2007b; Tye *et al.*, 2009; Matocha *et al.*, 2016). The K^+ demand by plants during growth periods has likewise been shown to cause the removal of K^+ from clay mineral interlayers and result in a higher abundance of expandable layers (Tributh *et al.*, 1987; Hinsinger, *et al.*, 1992; Velde and Peck, 2002; Barre *et al.*, 2007b). In the present study, a further proposal is made that, under slow growth periods (*i.e.*, root/microbe respiration without photosynthesis), water tables rise and dysaerobic or low oxygen conditions allow the reduction of octahedral ferric Fe and the fixation of K in interlayer sites, which then serve as a K refugium.

In mature natural forest landscapes, despite the lack of fertilizer additions, the surface clay mineral fraction tends to show an increased abundance of illite-like minerals (Tice *et al.*, 1996; Turpault *et al.*, 2008; Calvaruso *et al.*, 2009; Cornu *et al.*, 2012), but agricultural plots with no K^+ fertilization show a decreased abundance of illite-like minerals (Velde and Peck, 2002). One mechanism to concentrate K^+ in the surfaces of mature forests has been described as “nutrient uplift” (Jobbagy and Jackson, 2004; Barre *et al.*, 2007a, 2007b) wherein the primary minerals at depth are hydrolyzed and/or oxidized by tree roots and the associated fungal hyphae. These dissolved nutrients are transported to the above-ground plant biomass and are later deposited at the soil surface by litter fall. The decomposition of this litter fall results in increased nutrient concentrations in the surface soil, which are then incorporated into 2:1 layer phyllosilicates.

Following from these hypotheses, the intensive cotton farming of the mid-19th and early 20th centuries, poor agricultural practices, and little erosion control may have resulted in soils that are depleted in K^+ and are dominated by 1:1 phyllosilicates and Al and Fe (oxyhydr)oxides. Meanwhile, land that was maintained as hardwood plots and used for pastures (*i.e.* that were spared from clearing and intensive farming) would have maintained illite-like minerals near the surface *via* nutrient cycling in the natural system. With these endpoints established, an increase in illite-like minerals in a plot that was rehabilitated by planting pines, which was a common practice in the mid-20th century to control erosion, may be seen as evidence that the pre-colonist era of nutrient cycling has been re-established and suggests that the critical zone is progressing toward a state of sustainable cycling of elements.

One obstacle to identify these changes in clay mineralogy is the compositional subtlety, which has been often overlooked in X-ray diffraction (XRD) data. Several methods have been developed to examine XRD patterns in an attempt to identify these changes, which

include measuring the center of gravity of the illite-like mineral region in the XRD pattern (Barre *et al.*, 2007b), peak decomposition of XRD patterns (Lanson, 1997), and whole pattern fitting (Hubert *et al.*, 2009, 2012). This difficulty is especially relevant to the CCZO soils because of the dominance of kaolinite and hydroxy-interlayered vermiculite (HIV). The data presented in the present paper suggest that the majority of micaceous minerals that are available as a nutrient reservoir are mixed layer minerals that usually include various amounts of kaolinite-illite (K-I), illite-vermiculite (I-V) mixed layers, and minor amounts of kaolinite-smectite (K-S) and illite-smectite (I-S). Whole pattern fitting is the most rigorous quantitative method to identify mixed layer clays that contain more than two layer types or contain the same layer type with multiple hydration states (Viennet *et al.*, 2015), as is often the case in soils. An identification of all the extant hydration states for each expandable layer type is not needed to identify long-term changes in expandable layer concentrations because the hydration states likely change over much shorter time scales. With these limitations considered, NEWMOD2[®] (Yuan and Bish, 2010), which uses two-component mixing models, was used to model the oriented-clay fraction XRD patterns and quantify the illite-like layers. Although minor amounts of additional components may be present, the errors caused by this limitation can be minimized by modeling Mg-saturated, ethylene-glycol solvated (Mg-EG) clay slides and by assuming that this state represents a uniform interlayer cation spacing (Tye *et al.*, 2009). This modeling method was used to test the hypothesis that the pine forest soil clays will have a greater quantity of illite-like minerals near the surface than at depth and that the quantities of illite-like layers will be intermediate between the values in the old hardwood forest and the cultivated field soils.

FIELD SITE AND METHODS

All the field sites were located in the CCZO in the Sumter National Forest in Union County, South Carolina, USA. Soil cores were hand augered to obtain samples from three field plots with different land use histories. Soil cores were collected at 10-cm increments from 0–40 cm and at 20-cm increments, thereafter. All the plots were within one km of each other and were situated on the same broad, high-order interfluvium (Figure 1). The hardwood site was augered to a depth of 80 cm (34.606389 N; –81.723056 W, IGSN: IEJCA0004); the pine site was augered to 150 cm (34.606944 N; –81.723056, IGSN: IEJCA0005); and the cultivated field was augered to 300 cm (34.611111 N; –81.727778, IGSN: IEJCA0013). The parent materials were mapped as biotite-quartz-feldspar gneiss in the pine and hardwood plots (Whitmire Reentrant) and metadiorite in the cultivated plot (Wildcat Complex) (Horton and Dicken, 2001). Particle size analyses were performed on

separate cores collected adjacent to the cores described above. The cores were sieved to remove the >2 mm fraction, and the <50 μm and <2 μm fractions were separated in a single step using a settling tube (Figure 2). Based on field observations and the measured clay (wt.%) contents, the depths to the tops of the Bt horizons were shown to be 60 cm for the hardwood plot, 15 cm for the pine plot, and 13 cm for the cultivated plot.

The soil materials were subsampled, the >2 mm fractions were removed, and the remaining <2 mm materials were ultrasonically disaggregated using a Branson Sonifier Cell Disruptor 350 (Branson Sonic Power Company, Danbury, Connecticut, USA) in deionized water that contained 38 g/L hexametaphosphate (Alfa Aesar, Ward Hill, Massachusetts, USA) and 2 g/L sodium carbonate (Baker Chemical Co., Phillipsburg, New Jersey, USA). The <2 μm fractions were separated from the dispersed materials using standard settling techniques (Moore and Reynolds, 1997). The Mg^{2+} - and K^+ -saturated, <2 μm subsamples were prepared using MgCl_2 (Acros, Morris Plains, New Jersey, USA) and KCl (Fisher Chemical, Fairlawn, New Jersey, USA) by adding 5 successive aliquots of 0.1 M MgCl_2 or 1.0 M KCl, respectively. The Mg^{2+} - and K^+ -saturated samples were rinsed with deionized water after saturation to remove excess MgCl_2 or KCl.

Sedimented oriented clay slides (infinite X-ray thickness, >10 mg cm^{-2}) were prepared for X-ray diffraction (XRD) analyses by pipetting suspended clay onto petrographic slides and allowing the slides to dry overnight for the Mg-saturated (air-dried) and the Mg-EG treatments. The air-dried and EG solvated K-saturated slides (K-EG) were prepared using the “stick and peel” method described in Moore and Reynolds (1997).

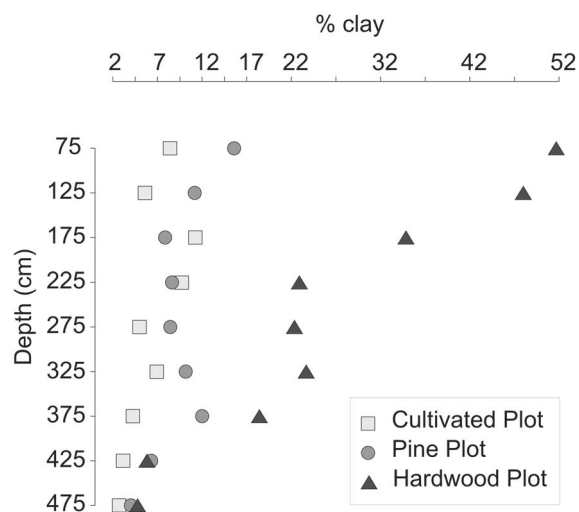


Figure 2. Measured %clay contents for soil samples from the cultivated, pine, and hardwood plots vs. profile depth.

Oriented clay slides were analyzed using a Bruker Advance D8[®] X-ray diffractometer (Bruker, Karlsruhe, Germany) using Fe-filtered Co $K\alpha$ radiation (40 kV, 40 mA). The Mg- and K-saturated clay slides were solvated with EG overnight at 25°C and scanned. Subsequent XRD scans were performed on the same slides after heating to 300°C and 500°C. All oriented clay slides were scanned from 2 to 70°2 θ using a step size of 0.01°2 θ , a scan speed of 0.3 s/step, and were recorded using a Bruker LynxEye[®] detector.

The LTSE plots have been historically sampled at intervals of between five and seven years from 1962 through 2017. These plots were farmed for cotton until the early 1950s. After purchase by the U. S. Forest Service, the fields were left fallow with minimal biomass for three years and were then planted with Loblolly Pine as part of a plant density study (Metz, 1958). The soils were sampled in layers that included the O1 and O2 surface horizons and then at intervals of 0–7.5 cm, 7.5–15 cm, 15–35 cm, and 35–60 cm. These samples were mixed together to make composite samples with 18–20 samples per 0.1 ha plot that were distinguished by the planting density and were randomly collected using a punch tube. Archived samples from 1964, 1997, and 2005 were mixed together to make composite samples across all plots, the <2 μm fractions were separated, and the samples were prepared for oriented-slide XRD using the methods described above. These soil samples were included to identify any changes in soil clay mineralogy that might have resulted from rapid pine growth through the decades. Elemental analyses of these soil samples by Bacon (2014) showed that exchangeable K^+ values decreased from about 20 kg/ha to <5 kg/ha between 1962 and 1997 and subsequently increased to 20 kg/ha in the 2007 samples from a 0–7.5 cm depth. A similar trend was observed in exchangeable K^+ in soil samples from the 7.5–15 cm depth, but with a narrower range in K^+ values. The range in K^+ values was relatively constant at a 35–60 cm soil depth over this time period. Biomass sampling over the same time period showed a corresponding biomass K increase from 0 to 250 kg/ha between 1960 and 1990 and a decrease to 150 kg/ha in 2007 (Bacon, 2014).

XRD patterns of oriented clay slides were analyzed to identify smectites based on the behavior of the 10–17 Å peaks in the K-EG samples (Moore and Reynolds, 1997). Mineral phases were identified using the basal d -spacing reflections as identified using XRD. Smectite, vermiculite, and hydroxy-interlayered vermiculite (HIV) were differentiated by comparing the Mg^{2+} - and K^+ -saturated sample XRD patterns of air-dried and Mg-EG and K-EG solvated samples and with K^+ -saturated samples heated to 110°C, 330°C, and 550°C. Kaolinite was identified by the 7.15 Å and 3.57 Å peaks. An asymmetry on the low angle side of the 7.15 Å peak was interpreted as kaolinite mixed-layered minerals (Hong *et al.*, 2012, 2015). Kaolinite-illite (K-I) was distinguished from kaolinite-

smectite (K-S) or kaolinite-vermiculite (K-V) by using the low angle portion of XRD patterns to identify the presence of smectite and from the absence of a shoulder on the low angle side of the 7.15 Å kaolinite (001) peak under Mg-EG and K-EG solvation. In ambiguous cases, the best model fit was used to distinguish K-I, K-V, and K-S. Illite was identified by a 10.0 Å peak that did not shift under any treatment. HIV was identified by a relatively narrow peak at 14.2 Å that did not collapse with K⁺ saturation nor expand with K-EG solvation. The 14.2 Å peak collapsed after heating to 330°C. Smectite was identified in Mg-saturated samples by an increase in the <5°2θ intensity. The <5°2θ intensity decreased with K⁺ saturation and the 10.0 Å peak intensity increased. Smectite was interpreted to be interlayered because no distinct peaks were identified in Mg²⁺-saturated air-dried or Mg-EG solvated samples. Similarly, vermiculite was identified by an increase in the intensity between 10 and 14°2θ and by the appearance of a broad peak superimposed on the relatively narrow 14.2 Å HIV peak. The intensities of the characteristic vermiculite peaks decreased and the 10.0 Å peak intensity increased with K⁺ saturation. Again, no distinct vermiculite peak was observed under any conditions and the vermiculite was interpreted to exist as interlayers mixed with illite.

The Mg-saturated and Mg-EG samples were modeled using NEWMOD2[®]. Simulations between 2 and 30°2θ were performed for various physical mixtures of both discrete and mixed-layer clay types after a linear background removal using parameters specific to the instrument and typical for clay minerals (Table 1). Using a forward modeling approach, variables for coherent-scattering domain-size distribution, layer type, layer type percentage, and ordering scheme (*i.e.* Reichweite) were adjusted to establish a best visual fit between the observed and the modeled data. Modeling one saturation state introduces a limitation that cannot easily be overcome. Multiple models of the same sample under different saturation states would serve to further constrain the models and allow for more confidence in

the uniqueness of the solutions presented. These multiple model comparisons were not included because an inconsistent sample response (*i.e.* incomplete layer collapse/expansion) under different treatments led to unique model solutions for most samples. In addition, K⁺-saturated sample models result in increased illite (modeled as trioctahedral mica) contents in the results. In order to most accurately identify the soil minerals, the Mg²⁺-saturated and Mg-EG samples were chosen as the most predictable XRD patterns to conserve the peaks for all the modeled minerals. The XRD patterns were visually inspected and the weighted-profile R factor (R_{wp}), expected R factor (R_{exp}), and goodness of fit (G) values were calculated for each model solution using the following equations (Toby, 2006):

$$R_{wp} = \sqrt{\frac{\sum_i w_i (y_{c,i} - y_{o,i})^2}{\sum_i w_i (y_{o,i})^2}} \quad (1)$$

$$R_{exp} = \sqrt{\frac{N}{\sum_i w_i (y_{o,i})^2}} \quad (2)$$

$$G = R_{wp}/R_{exp} \quad (3)$$

where y represents the intensity values, w represents the weight ($w = 1/\sigma^2[y_{o,i}]$, $\sigma^2[y_{o,i}] = y_{o,i}$) the subscript c indicates the calculated counts, and the subscript o indicates the measured counts for $i^{\circ}2\theta$.

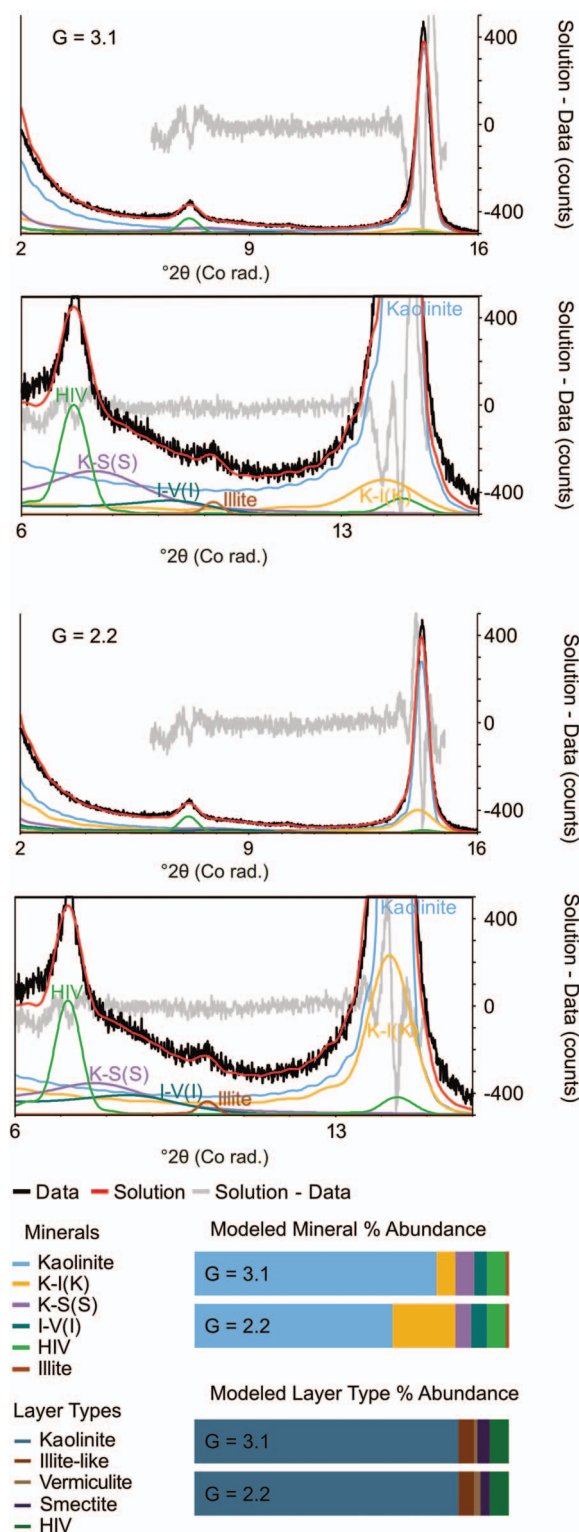
The goodness of fit G values were calculated between 6 and 15°2θ because the gibbsite and quartz peaks were not modeled using NEWMOD2[®]. Below 6°2θ, modeling the low angle portion of the profile was difficult, especially for samples with high kaolinite contents (Tye *et al.*, 2009). Best-fit models were identified by the combined use of a visual fit with a minimum goodness of fit value. Goodness of fit values ranged from 1.6 to 3.1 with an average value of 2.3 (Figure 3). Smectite was included in all sample solutions, where the behavior of the (001) reflection under multiple saturation treatments indicated expandable layers. Because non-unique solutions (*i.e.*, multiple model solutions that result in equivalent G values) are possible, three samples were randomly chosen for five successive model repetitions. These models were completed independently on different days to ensure that previous solutions did not influence subsequent model solutions.

For the purposes of this discussion, a distinction was made between minerals and layer types. Mineral abundance included discrete and mixed layer phases and were identified by layer types, *e.g.* kaolinite-illite (K-I) or illite-vermiculite (I-V). During modeling, the more abundant layer type was identified. In this case, K-I with more illite-like layers than kaolinite layers were referred to as illitic K-I or K-I (I). Layer type abundance represents the total abundance of a layer type summed across all discrete and mixed-layer clays in a sample that

Table 1. NEWMOD2[®] Parameter Values.

Parameter	Value
Radiation Wavelength (l)	1.7889
Divergent Slit	0.6
Goniometer Radius (cm)	21.75
Soller Slit 1	6.6
Soller Slit 2	2.5
Sample Length (cm)	1.5
Quartz Ref. Intensity (counts)	30000
Preferred Orientation (s*)	12
Absorption Coefficient (m star)	45
Exchange Capacity	0.36
Exchange Cation	Sample Specific
Theta Comp Slit Out	Checked
Random Powder (RNDPWD)	Checked

contains that layer type. The maximum standard deviation for the modeled abundance (wt.%) of a phase was 7.1% and the average standard deviation was 2.5%.



When the total number of each layer type was compared across the five models, the maximum standard deviation was 2.0% and the average standard deviation was 1.1% (Table 2). Based on these results, the modeled %mineral abundance values were considered to be accurate to within 8% and the sum of individual layer types to be accurate to within 2%.

The effect of summing layer types was demonstrated by comparing two solutions for sample GPP209 (pine plot, 120–140 cm) that appeared to be acceptable visual fits. The G values differed for the two model solutions (3.1 vs. 2.2) and the modeled abundance of K-I (K) (6 vs. 20%); the layer type abundances, however, were essentially identical. The model solution with the lower G value included more K-I (K) and had 99% kaolinite layers. The difference in the total number of illite-like layers that were added was negligible (e.g., Figures 3c and 3d).

RESULTS

The hardwood plot soil samples had the highest clay contents (52 wt.%) at depths between 50 and 100 cm. The clay contents of the pine and cultivated plots were much lower (17% and 9%, respectively) at the same depths (Figure 2). The clay contents of the hardwood plot samples decreased steadily, ranged from 22% to 17% between 200 and 400 cm, and then decreased to 5%. Clay contents in the pine plot samples decreased from 17% to 9% between 50 and 250 cm, increased to 12% between 250 and 400 cm, and then decreased to 5%. In the cultivated plot samples, clay contents increased to 12% between 150 and 200 cm and then decreased to 5% with greater depth (Figure 2).

The clay mineral composition of all three soil profiles was dominated by kaolinite. Across the study, the minimum modeled kaolinite abundance was 34% at the surface (0 to 10 cm) of the pine plot. In contrast, kaolinite contents at the surface in the hardwood and cultivated plots were 43% and 39%, respectively (Table 3, Figure 4). In the hardwood and pine plots, kaolinite abundance increased to 61% and 66% at depths between 0 and 60 cm, respectively. In the pine plot, the kaolinite abundance was constant between the depths of 60 and 160 cm. Kaolinite abundance in the cultivated plot decreased to 26% at a depth of 260 cm.

Figure 3. Two possible modeling solutions for the XRD patterns of pine plot (120–140 cm) soil clay samples are compared. The largest difference was between the K-I (K) contents estimated by the first ($G = 3.1$) and second ($G = 2.2$) modeling solutions. This illustrates the differences between goodness of fit (G) and visual fit (especially between $13^\circ 2\theta$ and $14^\circ 2\theta$). The mineral and layer type contents were also plotted to show the relatively large differences between the K-I (K) contents in the two modeling solutions, which did not appreciably change the proportions of illite-like and kaolinite layers.

Table 2. Summary of model variability in three random samples.

	Modeled % Abundance													
	K-I (K)		K-I (I)		Ill	I-V (I)		I-V (V)		K-S (S)		HIV	G	
Kao	K-I	%K	K-I	%K		I-V	%I	I-V	%I	K-S	%K			
<i>GPP202 n = 6</i>														
Min	54	7	0.92	5	0.25	0	8	0.66	3	0.31	0	0.00	5	3
Max	63	10	0.99	10	0.40	0	15	0.77	12	0.50	0	0.00	7	3
Average	58	9	0.97	7	0.32	0	13	0.72	7	0.36	0	0.00	6	3
Standard Deviation	3.2	1.2	0.03	2.0	0.07	0.0	2.7	0.04	3.2	0.07	0.0	0.00	0.7	0
<i>zGPP209 n = 6</i>														
Min	63	4	0.97	0	0.00	1	0	0.00	0	0.00	5	0.34	3	3
Max	75	20	0.99	0	0.00	2	5	0.69	2	0.39	12	0.50	8	3
Average	70	11	0.99	0	0.00	2	1	0.12	1	0.23	10	0.43	5	3
Standard Deviation	4.3	5.4	0.01	0	0.00	0.4	2	0.28	0.8	0.14	2.6	0.05	1.4	0
<i>DF007 n = 5</i>														
Min	35	31	0.92	10	0.36	0	5	0.67	0	0.00	0	0.00	1	2
Max	50	43	0.96	15	0.48	2	7	0.87	3	0.46	0	0.00	1	2
Average	42	37	0.94	12	0.42	1	7	0.73	1	0.17	0	0.00	1	2
Standard Deviation	6.4	4.9	0.02	1.9	0.05	0.8	0.9	0.08	1.7	0.24	0.0	0.00	0.3	0
Modeled % Layer Types														
	Kao	Illite	Vermiculite		Smectite		HIV							
<i>GPP202 n = 6</i>														
Min	67	14	7		0		5							
Max	72	19	9		0		7							
Average	69	17	8		0		6							
Standard Deviation	2.0	1.6	0.9		0		0.7							
<i>GPP209 n = 6</i>														
Min	84	2	1		3		3							
Max	87	5	2		6		8							
Average	85	3	1		5		5							
Standard Deviation	1.2	1	0.4		1.2		1.4							
<i>DF007 n = 5</i>														
Min	81	14	2		0		1							
Max	83	16	3		0		1							
Average	82	15	2		0		1							
Standard Deviation	0.7	0.8	0.3		0		0.3							

In the pine and cultivated plots, K-I was the second most abundant mineral, while K-I was only a minor fraction in the hardwood plot. The K-I (K) abundance decreased with depth in the hardwood plot and increased with depth in the pine and cultivated plots. The K-I (K) in the cultivated plot was modeled using >90% kaolinite layers throughout the profile. All kaolinite layers (*i.e.*, discrete kaolinite and K-I) summed to almost 80% kaolinite layers in the cultivated plot near the surface, trended to a maximum value of 92% at 60 cm, and then decreased to 57% at 220 cm. The maximum abundance of kaolinite layers in the hardwood and pine plot samples was 71% and 85%, respectively (Table 4, Figure 5).

The second most abundant mineral in the hardwood plot was I-V, which included both I-V (I) and I-V (V). The I-V content decreased in abundance from 33% near the surface to 15% at 70 cm. In the pine and cultivated plot surfaces, the I-V abundances were 27% and 9%, respectively. The I-V abundance in the pine plot

decreased with depth to a minimum of 5% at 80 cm. In the cultivated plot, the I-V content decreased to a minimum of 3% at 50 cm and then increased to 14% at 260 cm. Other low-abundance minerals modeled included K-S mixed layers, which occurred in the hardwood plot (60–80 cm) and the pine plot samples (80–160 cm). HIV was identified in all plots and K-V was only identified in the cultivated plot (180–200 cm).

The abundance of individual layer types decreased from 30% to 20% illite-like layers in the upper 60 cm of the hardwood plot, decreased in the pine plot from 30% to 10% between 0 and 60 cm, and decreased from 15% to 5% in the cultivated plot between 0 and 60 cm (Figure 5). Below 60 cm, the abundance of illite-like layers increased from 5% to 39% in the cultivated plot. No corresponding increase in mineral abundance occurred in the hardwood or pine plots. Kaolinite layer abundance increased with depth in the hardwood and pine plots and increased from 80% to 95% between 0

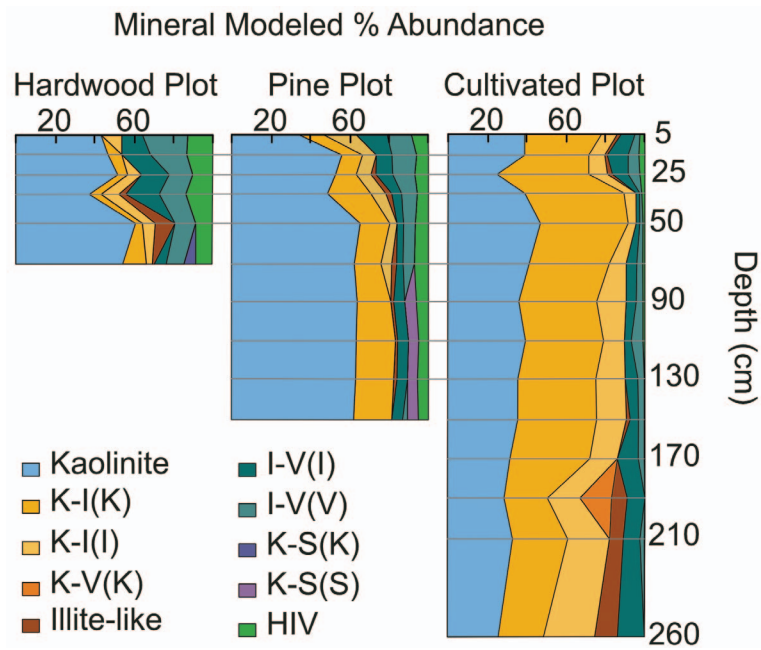


Figure 4. Modeled abundances (%) of clay minerals in the <2 μm fractions.

and 50 cm in the cultivated plot before decreasing to 57% with greater depth.

HIV was identified throughout the hardwood plot and the contents ranged from 13% to 9%. In the pine plot, HIV abundance was lower than in the hardwood plot and decreased with depth from 8% to 5%. In the cultivated plot, HIV decreased from a maximum of 3% between 10 and 20 cm depth and was not identified below 110 cm.

The modeled abundance of illite-like layers in the LTSE pine samples at the 7.5–15 cm depth interval decreased from 32% to 25% between 1960 and 1997. Variations in the illite-like layer contents remained within experimental error limits and were not statistically significant for all the other depth intervals. Kaolinite layer types increased through time in the 7.5–15 cm and 35–60 cm depth intervals. Kaolinite at

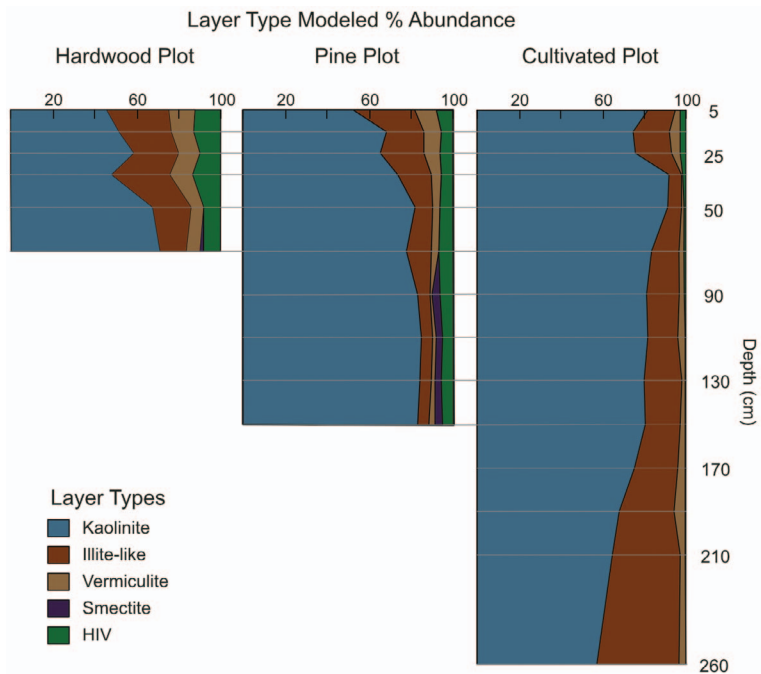


Figure 5. Modeled abundances (%) of layer types.

Table 3. Modeled %Abundance of clay-sized fraction clay minerals.

Sample	Depth range (cm)	Kao	Modeled %Abundance										Fitting Parameters					
			-K-I (K) - K-I % K	-K-I (I) - K-I % K	III	I-V	% I	-I-V (I) - % I	I-V	-I-V (V) - % I	K-S	% K	HIV	R _{wp}	R _{exp}	X2	G	
<i>Hardwood Plot (GHPXXX)</i>																		
201	0-10	43	0	0.00	11	0.18	0	10	0.95	23	0.50	0	0.00	13	0.17	0.50	8.3	2.9
202	10-20	47	7	0.69	0	0.00	15	0.89	18	0.50	0	0.00	13	0.15	0.32	4.3	2.1	
203	20-30	52	5	0.90	7	0.27	0	14	0.77	12	0.41	0	0.00	9	0.11	0.31	8.4	2.9
204	30-40	37	6	0.99	9	0.50	4	17	0.76	13	0.46	0	0.00	12	0.13	0.41	9.8	3.1
205	40-60	61	4	0.99	7	0.50	10	0	0.76	11	0.46	0	0.00	8	0.10	0.30	8.4	2.9
206	60-80	54	12	0.99	3	0.14	1	6	0.77	9	0.40	6	0.40	11	0.05	0.12	5.1	2.3
<i>Pine Plot (GPPXXX)</i>																		
201	0-10	34	12	0.95	17	0.34	0	15	0.77	12	0.50	0	0.00	8	0.10	0.29	8.0	2.8
202	10-20	56	10	0.97	7	0.25	0	8	0.77	12	0.50	0	0.00	6	0.06	0.18	8.1	2.8
203	20-30	53	10	0.97	7	0.25	2	9	0.81	12	0.50	0	0.00	7	0.08	0.18	5.2	2.3
204	30-40	49	22	0.99	7	0.34	3	5	0.74	8	0.50	0	0.00	6	0.07	0.17	5.4	2.3
205	40-60	66	15	0.99	3	0.34	0	4	0.74	6	0.50	0	0.00	6	0.05	0.13	6.1	2.5
206	60-80	62	13	0.99	6	0.34	3	3	0.74	6	0.50	0	0.00	7	0.06	0.15	7.2	2.7
207	80-100	64	17	0.99	0	0.00	2	5	0.74	0	0.00	6	0.34	6	0.05	0.11	4.7	2.2
208	100-120	64	20	0.99	0	0.00	1	6	0.74	0	0.00	5	0.34	5	0.04	0.10	5.1	2.3
209	120-140	63	20	0.99	0	0.00	1	5	0.69	0	0.00	5	0.34	6	0.04	0.09	4.9	2.2
210	140-160	62	19	0.99	0	0.00	0	6	0.69	2	0.50	5	0.28	5	0.04	0.11	6.0	2.5
<i>Cultivated Plot (DF0XX)</i>																		
01	0-10	39	39	0.99	8	0.47	2	7	0.76	2	0.50	0	0.00	2	0.05	0.09	3.1	1.8
02	10-20	42	29	0.99	8	0.41	1	10	0.76	6	0.50	0	0.00	3	0.06	0.09	2.8	1.7
03	20-30	25	47	0.99	9	0.50	2	8	0.83	6	0.50	0	0.00	2	0.05	0.08	2.5	1.6
04	30-40	39	51	0.99	6	0.50	0	2	0.83	1	0.50	0	0.00	1	0.05	0.10	3.9	2.0
05	40-60	47	45	0.97	4	0.28	0	2	0.78	1	0.50	0	0.00	1	0.05	0.09	4.0	2.0
06	60-80	42	41	0.95	8	0.37	0	6	0.87	3	0.50	0	0.00	1	0.05	0.09	3.8	2.0
07	80-100	36	40	0.95	15	0.48	0	5	0.87	3	0.46	0	0.00	1	0.05	0.11	4.5	2.1
08	100-120	40	40	0.94	10	0.50	0	4	0.92	6	0.49	0	0.00	0	0.06	0.11	3.2	1.8
09	120-140	35	40	0.94	15	0.50	0	7	0.92	3	0.49	0	0.00	0	0.05	0.10	3.6	1.9
10	140-160	36	40	0.94	15	0.50	2	4	0.84	3	0.49	0	0.00	0	0.05	0.10	4.0	2.0
11	160-180	32	41	0.91	14	0.46	0	10	0.84	3	0.45	0	0.00	0	0.05	0.11	4.5	2.1
12	180-200	23	28	0.92	16	0.40	8	9	0.76	0	0.00	16	0.21	0	0.07	0.19	7.2	2.7
13	200-220	33	28	0.84	21	0.38	7	8	0.86	2	0.46	0	0.00	0	0.07	0.17	5.9	2.4
14	220-300	26	23	0.90	27	0.42	11	14	0.77	0	0.00	0	0.00	0	0.07	0.13	3.3	1.8
													Min G	1.6				
													Max G	3.1				
													Average G	2.3				
													n	30				

Table 4. Table 4. Modeled %Abundance of layer types.

Sample	Depth range (cm)	Kaolinite	Illite	Vermiculite	Smectite	HIV
<i>Hardwood Plot (GHPXXX)</i>						
201	0–10	45	30	12	0	13
202	10–20	51	25	11	0	13
203	20–30	58	21	10	0	10
204	30–40	48	27	11	0	14
205	40–60	68	18	6	0	8
206	60–80	71	12	7	2	8
<i>Pine Plot (GPPXXX)</i>						
201	0–10	52	30	10	0	8
202	10–20	68	18	8	0	6
203	20–30	65	21	7	0	7
204	30–40	73	16	5	0	6
205	40–60	81	8	4	0	6
206	60–80	78	12	4	0	7
207	80–100	83	6	1	4	6
208	100–120	85	5	1	3	5
209	120–140	84	5	2	3	6
210	140–160	83	5	3	4	5
<i>Cultivated Plot (DF0XX)</i>						
01	0–10	82	15	3	0	2
02	10–20	75	17	5	0	3
03	20–30	76	18	4	0	2
04	30–40	92	6	1	0	1
05	40–60	92	5	1	0	1
06	60–80	84	14	2	0	1
07	80–100	81	16	3	0	1
08	100–120	82	14	3	0	0
09	120–140	81	17	2	0	0
10	140–160	81	17	2	0	0
11	160–180	75	21	4	0	0
12	180–200	68	33	5	0	0
13	200–220	65	33	2	0	0
14	220–300	57	39	3	0	0

other depth intervals and vermiculite and HIV abundances at all depths did not change significantly through time and no smectite layers were identified in these samples.

DISCUSSION

The experiments described above were conducted to test the hypothesis that the abundance of illite-like layers in the clay fraction of U.S. Piedmont soils was changed by land use history. More specifically, the intensely cultivated plots had fewer illite-like layers at the surface than did the pine forest plot that was previously cultivated. Furthermore, the abundance of illite-like layers was greatest near the surface in the hardwood plot that had no recent cultivation history and a long history of nutrient uplift by the forest.

The general trend of increased illite-like layer abundance at the surface (*i.e.*, 0–150 cm) supports the idea that increased K^+ input from biomass decomposition at the surface caused the storage of excess K^+ in the soil

mineral assemblage. Following deforestation, the rate of chemical denudation (*i.e.*, mineral mass lost in solution) was greater than the rate of chemical weathering (*i.e.*, transformation of primary to secondary minerals with the weathered mineral mass retained in plants, biomass, and clay minerals) (Balogh-Brunstad *et al.*, 2008). The mostly 1:1 clay mineral assemblage was dominant in the cultivated site. This resulted from a net loss of mass from the system, which is consistent with a higher chemical denudation rate in comparison to chemical weathering. The clay mineralogy of the pine site transitioned toward more illite-like mixed-layer minerals. During forest recovery, the chemical denudation rate was much slower than in the cultivated site and resulted in the net retention of mineral mass in the system. Differences in the denudation rates relative to weathering explain the mineral changes observed at the pine site relative to the cultivated site. Changes in the relative rates of these processes predict that a change will occur in the composition of the soil solutions. New dynamic chemical equilibria for each of the systems would then be possible.

This scenario was further supported by the LTSE archived soil data. Assuming that the nutrient uplift process is at work in the pine plot, the K^+ that was removed from minerals at depth as a result of increased biological demand during tree growth is deposited at the soil surface. As the plot matures from young to older trees and is managed by harvests, an increase in illite-like layer abundance is expected near the surface with a depletion of illite-like layers at depth over time. During biomass decomposition, the greatest change in illite-like mineral abundance is expected near the surface, while during periods of tree growth (*i.e.*, between 1960 and 1997) the abundance of illite-like layers are expected to decrease at depth (Figure 6). In fact, a decrease in illite-like layers occurred during the period of rapid tree growth between 1962 and 1997 in the 7.5–15 cm sample and no change at depths >15 cm. This suggests that roots in the shallow surface remove K^+ from clay minerals at relatively shallow soil depths during growth. All other changes in the abundance of illite-like layers were not significant.

Biomass measurements on this plot by Bacon (2014) showed that the K^+ concentrations in the biomass peaked in 1997. This correlates with the maximum depletion of illite-like layers in the 1997 sample and just below the surface in the 7.5–15 cm depth interval (Figure 6). The abundance of illite-like layers changed little below these shallow depths because Loblolly Pine are generally more deeply rooted than 60 cm (Richter and Markewitz, 1995). The change at the 7.5–15 cm depth may be explained by shallow roots that spread laterally above the Bt horizon at this depth. After 1997, the biomass declined in the plot. After 1997, no significant increase occurred in the wt.% illite-like layers, which is contrary to the hypothesized deposition of K^+ at the soil surface.

Changes in clay mineral composition suggest that the weathering profiles at each site are establishing states of “dynamic equilibrium” as defined by Hack (1960), whereby physical and chemical erosional energies result in down-wasting at the same rate through time. The clay mineral assemblages in each profile reflect differences in land use and vegetation changes through time for the

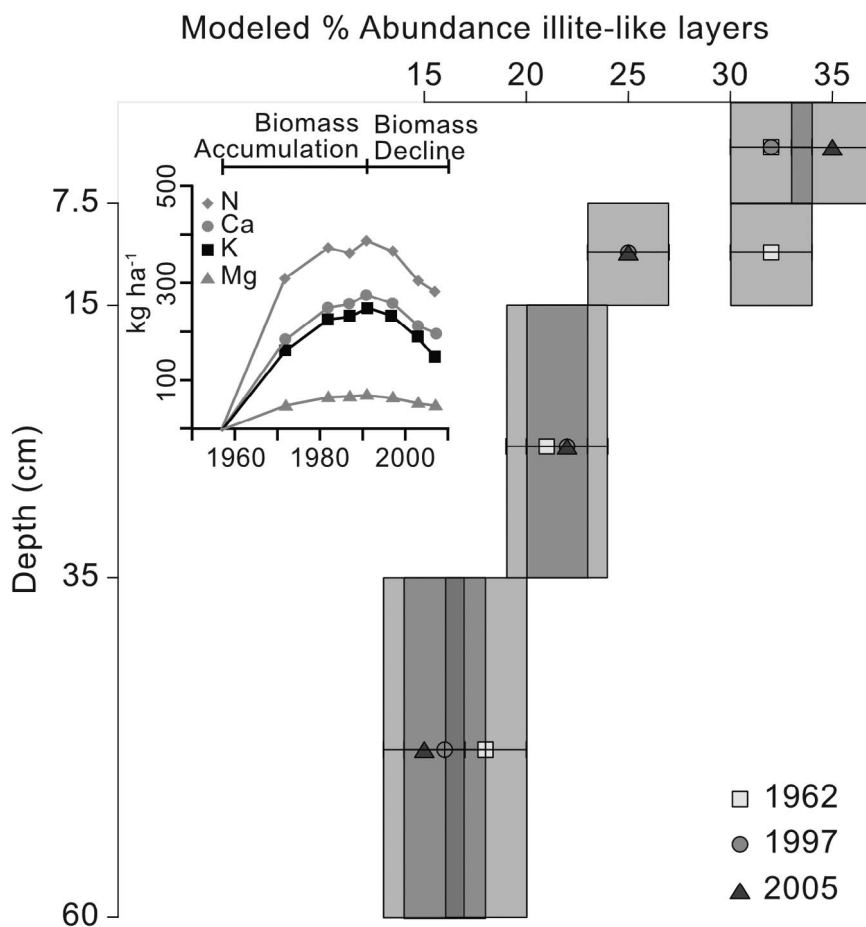


Figure 6. Modeled abundances (%) of illite-like layers in the LTSE soil samples. The error bars represent the $\pm 2\%$ level based on the analyses described in the text. The inset shows the total micronutrient contents of living pine biomass from 1957 to 2007 (Bacon, 2014).

past ~200 y. Physical changes are manifested in part by the removal of physical material *via* mass wasting erosion and in part by chemical reactions within each soil horizon.

Soil removal rates are influenced by plant types (*i.e.*, hardwoods *vs.* pines *vs.* grasses *vs.* no coverage) and tilling practices in the case of pine trees and crops (Chartier *et al.*, 2013). In plots with no cover or tillage, rainfall impact can remove fine particles from soil aggregates and result in the selective removal of the fine fraction (Palis *et al.*, 1997; Di Stefano and Ferro, 2002). An alternative hypothesis to explain the mineralogy differences between the three sites is, therefore, that the clay minerals are removed at different rates. The notable differences in clay abundance (wt.%) between the hardwood (52%) and the cultivated site (12%) illustrate that the erosion rates are different and that the clay removal rate at the cultivated site is faster than at the pine and hardwood sites. The differences in mineralogy might be explained by selective removal of the clay fraction or by physical erosion over more than a century of cultivation that included mechanical cultivation of the cultivated field during the last 80 y. Inverse relationships between the clay enrichment of legacy sediments have been found in the suspended solids in river loads, in flood plains, and in the clay contents of the upslope soils (Chartier *et al.*, 2013). These relationships suggest that, over time as the soil clay content is reduced, the aggregate stability is reduced and selective clay removal is enhanced. Restoration of the K⁺ nutrient reservoir in the form of illite-like layers in the pine plot would, therefore, be limited by diminished soil clay contents, which are expected to increase after tree cover slows the aggregate breakdown rate and clay-sized particle losses.

Selective clay removal by physical erosion may be an alternative explanation for the differences in clay mineralogy between the three sites. Kingery *et al.* (2002) compared the mineralogy of water-dispersible particles to the soil mineralogy and showed no statistically significant differences between the mica or HIV contents. If illite-like layers are preferentially removed during physical erosion, it follows that the rate of illite-like layer formation must be faster than erosion if the erosion rates of all clay mineral types are assumed to be equal.

CONCLUSIONS

Modeling XRD patterns using NEWMOD2[®] to obtain the clay mineral and layer type abundances as weight percentages has made possible a better understanding of the changes in these mineral assemblages that occur across landscapes with different plant management histories. The agricultural practices introduced by the end of the mid-19th century resulted in rapid erosion and increased denudation of mineral mass. Clay mineral assemblage differences were observed in

proximally located cultivated, pine, and hardwood sites. These conditions resulted in lower concentrations of K⁺ that shifted the kinetics of mineral transformation in the soil to favor kaolinite formation in the cultivated site. Pine forest regeneration from the 1950s to 2005 resulted in increased soil K⁺ concentrations, which favored more illite-like clay mineral formation. The pine site alterations have progressed from the surface downward through the soil profile on a decadal time scale, which indicates that relatively rapid mineral transformation is possible and supports the nutrient uplift hypothesis. While the pine site clay mineralogy was not regenerated to the assumed more “pristine” state of the hardwood site, the regeneration of a pool of exchangeable nutrients stored in the illite-like clay minerals at the surface indicates that a highly degraded Southeastern U.S. Piedmont soil is being restored to a more sustainable condition where pines have been planted.

ACKNOWLEDGMENTS

This work was supported by NSF grants EAR-GEO-1331846 and EAR-IF 0929912 and by a grant from the University of Georgia Department of Geology. Thanks to Paul Heine at Duke University Nicholas School of the Environment and anonymous reviewers whose thoughtful comments greatly improved the manuscript.

REFERENCES

- Bacon, A.R. (2014) *Pedogenesis and Anthropedogenesis on the Southern Piedmont*. Doctor of Philosophy PhD thesis. Duke University, Durham, NC. Bacon_duke_0066D_12361.pdf.
- Balogh-Brunstad, Z., Keller, C.K., Bormann, B.T., O'Brien, R., Wang, D., and Hawley, G. (2008) Chemical weathering and chemical denudation dynamics through ecosystem development and disturbance. *Global Biogeochemical Cycles*, **22**, <https://doi.org/10.1029/2007GB0022957>.
- Barre, P., Montagnier, C., Chenu, C., Abbadie, L., and Velde, B. (2008a) Clay minerals as a soil potassium reservoir: Observation and quantification through X-ray diffraction. *Plant and Soil*, **302**, 213–220.
- Barre, P., Velde, B., and Abbadie, L. (2007a) Dynamic role of “illite-like” clay minerals in temperate soils: Facts and hypotheses. *Biogeochemistry*, **82**, 77–88.
- Barre, P., Velde, B., Catel, N., and Abbadie, L. (2007b) Soil-plant potassium transfer: Impact of plant activity on clay minerals as seen from X-ray diffraction. *Plant and Soil*, **292**, 137–146.
- Barre, P., Velde, B., Fontaine, C., Catel, N., and Abbadie, L. (2008b) Which 2:1 clay minerals are involved in the soil potassium reservoir? Insights from potassium addition or removal experiments on three temperate grassland soil clay assemblages. *Geoderma*, **146**, 216–223.
- Calvaruso, C., Mareschal, L., Turpault, M.P., and Leclerc, E. (2009) Rapid clay weathering in the rhizosphere of Norway spruce and oak in an acid forest ecosystem. *Soil Science Society of America Journal*, **73**, 331–338.
- Chartier, M.P., Rostagno, C.M., and Videla, L.S. (2013) Selective erosion of clay, organic carbon and total nitrogen in grazed semiarid rangelands of northeastern Patagonia, Argentina. *Journal of Arid Environments*, **88**, 43–49.
- Cook, C.W., Brecheisen, Z., and Richter, D. (2015) *Calhoun CZO - Vegetation - Tree Survey (2014-2017)*. <http://criticalzone.org/calhoun/data/dataset/4614/>.

- Cornu, S., Montagne, D., Hubert, F., Barre, P., and Caner, L. (2012) Evidence of short-term clay evolution in soils under human impact. *Comptes Rendus Geoscience*, **344**, 747–757.
- Di Stefano, C. and Ferro, V. (2002) Linking clay enrichment and sediment delivery processes. *Biosystems Engineering*, **81**, 465–479.
- Hack, J.T. (1960) Interpretation of erosional topography in humid temperate regions. *American Journal of Science*, **258**, 80–97.
- Hinsinger, P., Jaillard, B., and Dufey, J.E. (1992) Rapid weathering of a trioctahedral mica by the roots of ryegrass. *Soil Science Society of America Journal*, **56**, 977–982.
- Hong, H., Cheng, F., Yin, K., Churchman, G.J., and Wang, C. (2015) Three-component mixed-layer illite/smectite/kaolinite (I/S/K) minerals in hydromorphic soils, South China. *American Mineralogist*, **100**, 1883–1891.
- Hong, H., Churchman, G.J., Gu, Y., Yin, K., and Wang, C. (2012) Kaolinite-smectite mixed-layer clays in the Jiujiang red soils and their climate significance. *Geoderma*, **173**, 75–83.
- Horton, J.W. and Dicken, C.L. (2001) *Preliminary Digital Geologic Map of the Appalachian Piedmont and Blue Ridge, South Carolina Segment*. U. S. Geological Survey. <https://geo-nstdi-er.usgs.gov/metadata/open-file/01-298/>.
- Hubert, F., Caner, L., Meunier, A., and Ferrage, E. (2012) Unraveling complex <2 μm clay mineralogy from soils using X-ray diffraction profile modeling on particle-size sub-fractions: Implications for soil pedogenesis and reactivity. *American Mineralogist*, **97**, 384–398.
- Hubert, F., Caner, L., Meunier, A., and Lanson, B. (2009) Advances in characterization of soil clay mineralogy using X-ray diffraction: From decomposition to profile fitting. *European Journal of Soil Science*, **60**, 1093–1105.
- Jobbagy, E.G. and Jackson, R.B. (2004) The uplift of soil nutrients by plants: Biogeochemical consequences across scales. *Ecology*, **85**, 2380–2389.
- Kingery, W.L., Han, F.X., Shaw, D.R., Gerard, P.D., and McGregor, K.C. (2002) Mineralogical and organic carbon content of water-dispersible particles from conventional and no-tillage soils. *Communications in Soil Science and Plant Analysis*, **33**, 947–961.
- Lanson, B. (1997) Decomposition of experimental X-ray diffraction patterns (profile fitting): A convenient way to study clay minerals. *Clays and Clay Minerals*, **45**, 132–146.
- Markewitz, D. and Richter, D.D. (2000) Long-term soil potassium availability from a Kanhapludult to an aggregating Loblolly pine ecosystem. *Forest Ecology and Management*, **130**, 109–129.
- Matocha, C.J., Grove, J.H., Karathanasis, T.D., and Vandiviere, M. (2016) Changes in soil mineralogy due to nitrogen fertilization in an agroecosystem. *Geoderma*, **263**, 176–184.
- Metz, L.J. (1958) The Calhoun Experimental Forest. Pp. 24. in: *Miscellaneous Publication, USDA U.S. Forest Service, Southern Research Station, Asheville, North Carolina, U.S.A.*
- Moore, D.M. and Reynolds, R.C., Jr. (1997) *X-ray Diffraction and the Identification and Analysis of Clay Minerals*. 2nd Edition. Pp. 378. Oxford University Press, New York.
- NCALM. National Center for Airborne Laser Mapping (2016) Leaf-off LiDAR Survey of the Calhoun Critical Zone Observatory. <http://opentopo.sdsc.edu/datasetMetadata?otCollectionID=OT.072016.26917.2>.
- Officer, S.J., Tillman, R.W., Palmer, A.S., and Whitton, J.S. (2006) Variability of clay mineralogy in two New Zealand steep-land topsoils under pasture. *Geoderma*, **132**, 427–440.
- Palis, R.G., Ghandiri, H., Rose, C.W., and Saffigna, P.G. (1997) Soil erosion and nutrient loss. III. Changes in the enrichment ratio of total nitrogen and organic carbon under rainfall detachment and entrainment. *Australian Journal of Soil Research*, **35**, 891–905.
- Pernes-Debuysse, A., Pernes, M., Velde, B., and Tessier, D. (2003) Soil mineralogy evolution in the INRA 42 Plots Experiment (Versailles, France). *Clays and Clay Minerals*, **51**, 577–584.
- Richter, D.D. and Markewitz, D. (1995) How deep is soil? *BioScience*, **45**, 600–609.
- Richter, D.D. and Markewitz, D. (2001) *Understanding Soil Change: Soil Sustainability Over Millennia, Centuries, and Decades*. Pp. 255. Cambridge University Press, Cambridge and New York.
- Tice, K.R., Graham, R.C., and Wood, H.B. (1996) Transformations of 2:1 phyllosilicates in 41-year-old soils under oak and pine. *Geoderma*, **70**, 49–62.
- Toby, B.H. (2006) R factors in Rietveld analysis: How good is good enough? *Powder Diffraction*, **21**, 67–70.
- Tributh, H., Vonboguslawski, E., Vonlieres, A., Steffens, D., and Mengel, K. (1987) Effect of potassium removal by crops on transformation of illitic clay-minerals. *Soil Science*, **143**, 404–409.
- Turpault, M.P., Righi, D., and Uterano, C. (2008) Clay minerals: Precise markers of the spatial and temporal variability of the biogeochemical soil environment. *Geoderma*, **147**, 108–115.
- Tye, A.M., Kemp, S.J., and Poulton, P.R. (2009) Responses of soil clay mineralogy in the Rothamsted classical experiments in relation to management practice and changing land use. *Geoderma*, **153**, 136–146.
- Velde, B. and Peck, T. (2002) Clay mineral changes in the Morrow Experimental Plots, University of Illinois. *Clays and Clay Minerals*, **50**, 364–370.
- Viennet, J.C., Hubert, F., Ferrage, E., Tertre, E., Legout, A., and Turpault, M.P. (2015) Investigation of clay mineralogy in a temperate acidic soil of a forest using X-ray diffraction profile modeling: Beyond the HIS and HIV description. *Geoderma*, **241**, 75–86.
- Yuan, H. and Bish, D.L. (2010) Newmod plus, a new version of the Newmod program for interpreting X-ray powder diffraction patterns from interstratified clay minerals. *Clays and Clay Minerals*, **58**, 318–326.

(Received 28 August 2017; revised 31 January 2018; Ms. 1198; AE: S. Kadir)